Journal of Solid State Chemistry 181 (2008) 3103–3109

Contents lists available at ScienceDirect

Journal of Solid State Chemistry

journal homepage: www.elsevier.com/locate/jssc

Synthesis, structures and magnetic properties of the new vanadates $AgMnVO_4$ and $RbMnVO_4$

Hamdi Ben Yahia, Etienne Gaudin *, Jacques Darriet

CNRS, Université de Bordeaux, ICMCB, 87 Avenue du Dr. A. Schweitzer, Pessac F-33608, France

ARTICLE INFO

Article history:
Received 28 May 2008
Received in revised form
28 July 2008
Accepted 3 August 2008
Available online 7 August 2008

Keywords:
Vanadate
Stuffed-tridymite
Maricite
Merohedral twinning
Canted antiferromagnetism

ABSTRACT

The new compounds, $AgMnVO_4$ and $RbMnVO_4$ have been synthesized by solid state reaction route. Their crystal structures were determined from single-crystal X-ray diffraction data for $RbMnVO_4$ and powder X-ray diffraction data for $AgMnVO_4$. $AgMnVO_4$ crystallizes with the maricite-type structure in space group *Pnma*, $a = 9.5778(6)$ Å, $b = 6.8518(4)$ Å, $c = 5.3734(3)$ Å and $Z = 4$. $RbMnVO_4$ crystallizes in space group $P6_3$ with a stuffed tridymite-type structure, $a = 11.2584(3)$, $c = 8.9893(13)$ Å and $Z = 8$. A merohedral twinning was taken into account for its structural refinement. To our knowledge this is the first vanadate showing this structural type. $AgMnVO_4$ and $RbMnVO_4$ were characterized by magnetic susceptibility and specific heat measurements. $AgMnVO_4$ is antiferromagnetic with a Néel temperature of 12.3 K determined by specific heat measurements. $RbMnVO_4$ exhibits canted antiferromagnetism with a Néel temperature of 6.5 K.

1. Introduction

Many compounds with general formula $ABPO_4$ (A = alkali metal, Cu, Ag; B = alkaline earth, transition metals) have been studied in the past. Theses phosphates mainly crystallize with four different structural types, i.e. olivine, maricite, stuffed-tridymite or zeolite-ABW. The stuffed-tridymite or zeolite-ABW structure types are observed with large alkali metal such as K, Rb or Cs. These alkali metals are located into the channels and they act as a template. In these structures the transition metal is mainly found in tetrahedral sites but is also sometimes observed in trigonal bipyramids. In the more condensed phases with olivine or maricite-type structures the transition metal is located in an octahedral site. We were interested to compare the structural evolution between homologous phosphates and vanadates and for this the series $AMnPO_4$ and $AMnVO_4$ have been chosen. In the $AMnPO_4$ phosphates series $LiMnPO_4$ [1], $NaMnPO_4$ [2], $KMnPO_4$ [3], $CsMnPO_4$ [4] were studied in the past and their structures determined. Recently we have reported the structural and magnetic characterization of $RbMnPO_4$ [5]. In the case of the homologous $AMnVO_4$ vanadates only $LiMnVO_4$ was known [6]. This compound crystallizes with the Na_2CrO_4-type structure whereas $LiFePO_4$ crystallizes with the olivine-type structure. This induces that on contrary to $LiFePO_4$ this compound is not interesting as cathode material for rechargeable Li-ion batteries [7]

Recently we have extended the $AMnVO_4$ vanadate series with $CuMnVO_4$ [8] and $KMnVO_4$ [9]. $CuMnVO_4$ crystallizes with the Na_2CrO_4 structure and contains MnO_4 chains made up of edge-sharing MnO_6 octahedra. Antiferromagnetic interactions in the chains and between the chains MnO_4 were evidenced. A surprising result was observed for $KMnVO_4$. Indeed, this compound crystallizes with a new type of oxygen-deficient perovskite. Antiferromagnetic interactions between Mn^{2+} ions were observed.

To complete the $AMnVO_4$ series, we have synthesized the new compounds $AgMnVO_4$ and $RbMnVO_4$ and studied their structural and magnetic properties.

2. Experimental

2.1. Synthesis

Powder samples of $AgMnVO_4$ were prepared by direct solid state reaction from stoichiometric mixtures of Ag_2O, MnO and V_2O_5 powders. The mixtures were fired at 500 °C in argon atmosphere for 2 days and heated at 700 °C for 36 h with intermediate grindings to ensure a total reaction. The progress of the reactions was followed by powder X-ray diffraction. At the end of the synthesis process the $Mn_2V_2O_7$ phase was detected as small impurity. To ensure that this is not due to the volatilization of Ag_2O, further synthesis were performed in sealed tube but $Mn_2V_2O_7$ was still found as impurity even if a small excess of Ag_2O

* Corresponding author. Fax: +33 5 4000 2761.
E-mail address: gaudin@icmcb-bordeaux.cnrs.fr (E. Gaudin).

0022-4596/$ - see front matter © 2008 Elsevier Inc. All rights reserved.
doi:10.1016/j.jssc.2008.08.001

is introduced. $Mn_2V_2O_7$ is very stable and was often observed during the synthesis of $AMnVO_4$ compounds. The lowest amount of $Mn_2V_2O_7$ was obtained by using a small excess of Ag_2O but a small amount of $AgVO_3$ was then observed even after several heat treatments (Fig. 1). This last sample with the lowest amount of impurities was chosen for the structural and physical characterizations. Attempts to get single crystals by melting the $AgMnVO_4$ powder were unsuccessful and led to the growth of single crystals of $Mn_2V_2O_7$ and Ag_2O.

$RbMnVO_4$ was synthesized by standard solid state method from $RbVO_3$ and MnO ($RbVO_3$ was obtained by heating a 1:1 mixture of Rb_2CO_3 and V_2O_5 at 600 °C for 10 h under O_2 atmosphere). The mixture was put in a gold tube, which was placed into a silica tube sealed under vacuum and then heated at 500 °C for 12 h. After grinding a further heating of the mixture at 650 °C for 24 h leads to a mixture of $RbVO_3$, $RbMnVO_4$ and a non-identified phase. Several heating treatments (with and without quenching) were tested to ensure a total reaction but a mixture of phases was always obtained. As $RbVO_3$ is soluble in water a last attempt using a 10% excess of $RbVO_3$ led us to obtain a powder of $RbMnVO_4$ after washing it with a very small amount of the unknown impurity (less than 2%) (Fig. 2). By heating of this starting mixture at 950 °C and then by slowly decreasing the temperature at the rate of 5 °C h^{-1} to room temperature a mixture of yellow, white, dark green and yellow-green crystals was obtained. They correspond to $RbMnVO_4$, $RbVO_3$, MnO and $Rb_2MnV_2O_7$ [10] phases, respectively.

2.2. X-ray diffraction, magnetic and specific heat measurements

To solve the crystal structure of $AgMnVO_4$ a high precision X-ray powder diffraction measurement was performed. The data were collected at room temperature over the 2θ angle range $5° \leqslant 2\theta \leqslant 150°$ with a step size of 0.02 ° using a Philips X-pert diffractometer operating with Cu$K\alpha$1 radiation. Dicvol [11] was used for the determination of the orthorhombic symmetry and a full pattern matching refinement was performed with the JANA2000 program package [12] The background was estimated by a Legendre function, and the peak shapes were described by a pseudo-Voigt function. The refinement of peak asymmetry was performed using four Berar-Baldinozzi parameters [13]. The 2θ zones $27 < 2\theta < 30.3°$ and $37.9 < 2\theta < 38.4°$ corresponding to impurities traces (Fig. 1) were excluded during the Rietveld refinement.

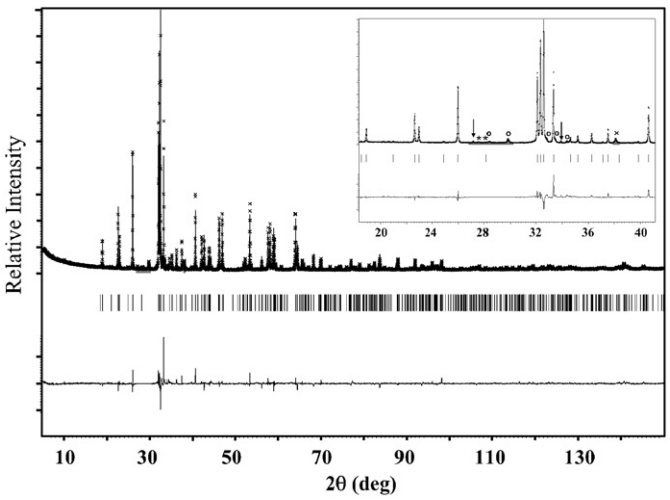

Fig. 1. Observed (crosses) and calculated (solid line) powder pattern of $AgMnVO_4$ after Rietveld refinement. The tick marks indicate the reflection positions and the difference plot is shown below. In the inset * corresponds to $Mn_2V_2O_7$, ° to $AgVO_3$ phases, × to silver metal and the arrows to unknown impurity.

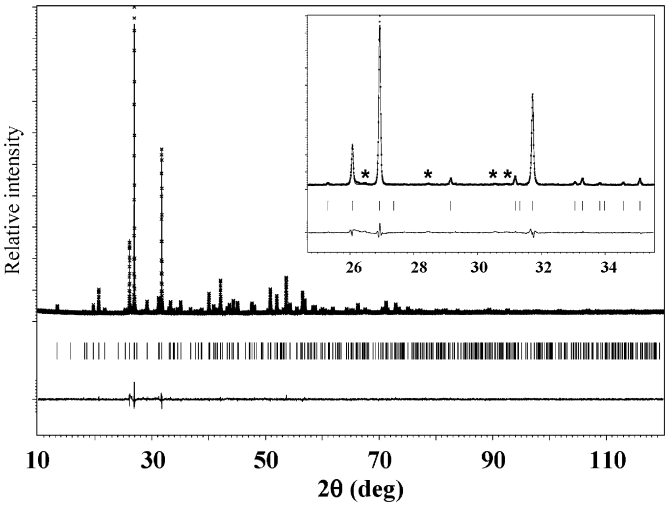

Fig. 2. Observed (crosses) and calculated (solid line) powder pattern of $RbMnVO_4$ after profile refinement. The tick marks indicate the reflection positions and the difference plot is shown below. * corresponds to the impurities as traces.

Single crystals of $RbMnVO_4$ suitable for X-ray diffraction were selected on the basis of the size and the sharpness of the diffraction spots. Most of the tested crystals were of poor quality and/or twinned. The data collection was carried out on an Enraf-Nonius Kappa CCD diffractometer using Mo$K\alpha$ radiation. Data processing and all refinements were performed with the JANA2000 program package [12]. A Gaussian-type absorption correction was applied, and the shape was determined with the video microscope of the Kappa CCD. It can be noticed that after absorption correction the averaging of the symmetry-equivalent reflections led to a relatively high value of the reliability factor R_{int}. This can be correlated to the quality of the crystal and the existence of twin domains.

Magnetic susceptibility measurements of polycrystalline samples of $AgMnVO_4$ and $RbMnVO_4$ were carried out with a Quantum Design SQUID magnetometer. The susceptibility versus T of $AgMnVO_4$ was calculated from the magnetization measurements at 5 kOe. It has been checked that the dependence of the magnetization versus field is linear at 2 K. In the range 2–60 K the susceptibility values were deduced from the slope of the $\sigma_{mol} = f(H)$ curves at $H = 5$ kOe and above 60 K directly from the magnetization values measured at the same field. For both studies diamagnetic corrections were carried out on the basis of Pascal's tables [14]. Heat capacity measurements were performed on $AgMnVO_4$ and $RbMnVO_4$ pellets using a PPMS Quantum Design in a temperature range from 2 to 100 K (Table 1).

2.3. Refinement

For $AgMnVO_4$ the X-ray diffraction pattern was indexed on the basis of an orthorhombic unit cell with the parameters $a = 9.5778(6)$, $b = 6.8518(4)$, $c = 5.3734(3)$ Å. Observed reflections and systematic extinctions are compatible with the space groups *Pnma* and $Pn2_1a$. The refinements were performed taking into account the centrosymmetric space group *Pnma*. The atomic positions of $AgCdVO_4$ were used as a starting model for the Rietveld analysis. After refinement of all atomic positions with isotropic atomic displacement parameters (ADP), the profile factors converged to the values $R_p/R_{wp} = 7.04/9.79\%$ and

Table 1
Crystallographic data and structure refinement for $RbMnVO_4$

Formula	$RbMnVO_4$
Crystal color	Yellow
MW ($g\,mol^{-1}$)	255.3
Crystal system	Hexagonal
Space group	$P6_3$
Cell parameters	$a = 11.2584(3)$ Å
	$c = 8.9893(13)$ Å
V(Å^3)	986.76(15)
Z	8
Density calc. ($g\,cm^{-3}$)	3.436(5)
Crystal shape	Block
Crystal size (mm)	$0.04 \times 0.03 \times 0.02$
Temperature (K)	293
Diffractometer	Enraf-Nonius Kappa CCD
Radiation	Mo$K\alpha$ ($\lambda = 0.71069$ Å)
$h\,k\,l$ range	$-15<h<15$ $-15<k<15$ $-12<l<12$
θ_{max}	30°
Linear absorption coeff.	$14.147\,mm^{-1}$
Absorption correction	Gaussian
T_{min}/T_{max}	0.610/0.762
No of reflections	17967
R_{int}	0.115
No of independent reflections	1923
Reflections used ($I>2\sigma(I)$)	1500
Refinement	F^2
$F(000)$	936
R factors $R(F)$/w$R(F^2)$	0.0411/0.0813
No. of refined parameters	87
g.o.f.	1.08
Weighting scheme	$w = 1/(\sigma^2(I)+0.0016I^2)$
Diff. Fourier residues (e^-/Å^3)	[−1.22; +1.21]
Twin fractions[a]	0.35(4), 0.56(3), 0.0(2), 0.08(2)

[a] The matrix of the twin elements are (100,010,001), ($\bar{1}$10,010,001), ($\bar{1}$00,0$\bar{1}$0,00$\bar{1}$), (1$\bar{1}$0,0$\bar{1}$0,00$\bar{1}$) with the notation used in JANA2000 [11].

Table 2
Atomic positions and isotropic displacement parameters for $AgMnVO_4$

Atoms	Site	x	y	z	U_{iso}(Å^2)
Ag	4c	0.3500(4)	1/4	0.0022(13)	0.0253(14)
Mn	4a	1/2	1/2	1/2	0.014(2)
V	4c	0.6802(8)	1/4	0.024(3)	0.017(3)
O1	4c	0.855(3)	1/4	0.044(7)	0.024(10)
O2	4c	0.634(4)	1/4	−0.281(5)	0.022(9)
O3	8d	0.612(3)	0.454(3)	0.167(4)	0.021(8)

$\chi^2 = 4.31$. In the final stage of the refinement a preferential orientation along the (010) direction was taken into account and improved significantly the reliability factors to $R_p/R_{wp} = 6.49/8.96\%$ and $\chi^2 = 3.63$. Fig. 1 shows the agreement between the calculated and observed profiles for $AgMnVO_4$. The final atomic positions and isotropic ADPs are displayed in Table 2.

The extinction conditions observed for $RbMnVO_4$ agree with the space group $P6_3$, $P6_3/m$ and $P6_322$. By analogy with the structural determination of isotypic phases the non-centrosymmetric space group $P6_3$ was used at the beginning of the refinement. This choice was confirmed at the end of the refinement. Most of the atomic positions were found by direct method using the sir97 program [15]. The use of difference-Fourier synthesis allowed us to localize the remaining oxygen atom positions. With anisotropic displacement parameters for all positions, the residual factors converged to the value $R(F) = 0.0873$ and w$R(F^2) = 0.2154$ for 84 refined parameters, 1500 observed reflections and difference-Fourier residues in the range between 2.51 and +1.25 e Å^{-3}. At this stage of the refinement some oxygen positions exhibited non-positive definite ADP matrix with very high U^{ij} values.

Table 3
Atomic positions and equivalent isotropic displacement parameters for $RbMnVO_4$

Atomes	X	y	z	U_{eq}(Å^2)
Rb1	0.47493(13)	0.51665(13)	0.4005	0.0281(4)
Rb2	0	0	0.3832(2)	0.0282(4)
Mn1	1/3	2/3	0.0677(2)	0.0183(6)
Mn2	0.32938(14)	0.1655(2)	0.2030(2)	0.0201(8)
V1	0.1602(2)	0.3323(2)	0.0965(2)	0.0156(7)
V2	2/3	1/3	0.1574(3)	0.0204(7)
O1	0.1791(7)	0.1934(7)	0.1238(8)	0.028(3)
O2	0.5032(6)	0.2712(8)	0.0899(7)	0.030(3)
O3	0.3335(7)	0.2199(7)	0.4150(9)	0.033(3)
O4	2/3	1/3	0.3443(13)	0.047(3)
O5	0.3091(7)	0.4831(7)	0.1333(7)	0.026(3)
O6	0.0299(7)	0.3200(8)	0.2070(7)	0.032(3)

Twinning by merohedry is often observed in hexagonal systems and for instance Kahlenberg et al. [16] have refined the structure of the stuffed-tridymite $BaGa_2O_4$ by considering the space group $P6_3$ and the twin element $2_{[110]}$. Taking into account a merohedral twinning one may consider the two Laue classes of the hexagonal system 6/m and 6/mmm. The point group 6 corresponds to the space group $P6_3$ and is a subgroup of index 2 of 6/m. In this case the twinning can be described by the introduction of the inversion centre as twin element (racemic twin). This has been tested with the refinement of the Flack parameter but the refinement was not really improved. Then the Laue class 6/mmm has been considered for the determination of the twin elements. $P6_3$ is a subgroup of index 4 of 6/mmm then four twin laws should be considered. In the software JANA2000 [12] a procedure to decompose a point group into cosets with respect to a subgroup is implemented. In our case the point group 6/mmm has been decomposed into four cosets and we have chosen one representative symmetry elements for three of them, the first one being the identity element. For one coset whatever the choice of the representative symmetry element the same twin fraction is expected at the end of the refinement. The following twin elements have been chosen: $m_{[100]}$, the inversion centre and $2_{[100]}$. As a merohedral twinning has been considered all the symmetry elements of the space group $P6_3$ can be used for merging symmetry-equivalent reflections [17]. The refinement of the fractional volumes of the twin domains led to the values 0.35(4), 0.56(3), 0.0(2), 0.08(2) for the twin elements E, $m_{[100]}$, i, $2_{[100]}$, respectively. This result means that the crystal is mainly composed of two twin domains. In our case the major domain is described by the twin law $m_{[100]}$. At the end of the refinement the residual factors converged to the values $R(F) = 0.0411$ and w$R(F^2) = 0.0813$ for 87 refined parameters, 1500 observed reflections and difference-Fourier residues in the range between −1.22 and +1.21 e Å^{-3}. The ADPs matrices of all the oxygen positions are now positive-definite with reasonable values of the U^{ij} components. The refined atomic positions and anisotropic ADPs for $RbMnVO_4$ are given in Table 3 and Supplementary materials, respectively.

3. Results and discussion

3.1. Crystal structure

3.1.1. $AgMnVO_4$

$AgMnVO_4$ crystallizes with the maricite-type structure. The structure consists of edge-sharing chains of MnO_6 octahedra running parallel to the b axis. These chains are connected between

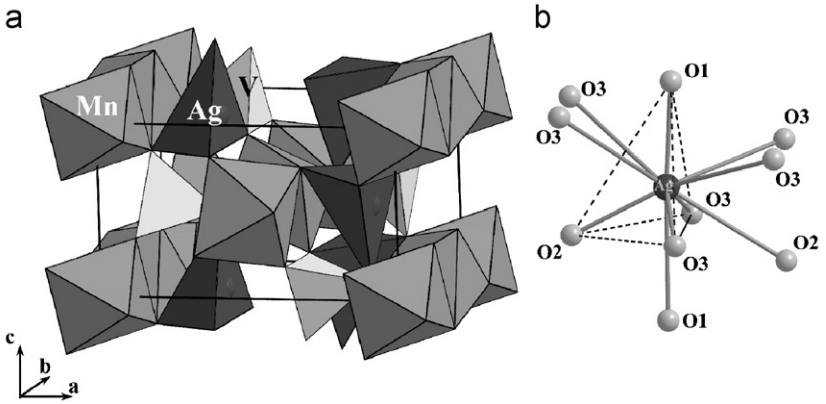

Fig. 3. (a) Perspective view of $AgMnVO_4$ structure and (b) surrounding of silver atoms.

them by VO_4 tetrahedra (Fig. 3a). The MnO_6 and VO_4 polyhedra are sharing corner and the silver atoms are located in strongly distorted tetrahedral site (Fig. 3b). These tetrahedra are sharing corners with the MnO_6 and VO_4 polyhedra. Interatomic distances and bond valence sums are given in Table 4.

The distances Mn–O range from 2.11 to 2.44 Å with an average distance of 2.26 Å. These distances are very similar to those observed in the $NaMnPO_4$ structure where the distances Mn–O range from 2.077 to 2.397 Å with an average distance of 2.229 Å [2]. The VO_4 tetrahedron is quite regular with distances ranging from 1.68 to 1.72 Å and an average value of 1.70 Å. The Ag^+ ion is located in a strongly distorted tetrahedron made of oxygen atoms belonging to four different MnO_6 octahedra (Fig. 3b). The O–Ag–O angles range from 86.5° to 128.5° and the average Ag–O distance is 2.33 Å which is comparable to the average distances of 2.391(1) and 2.374(3) Å observed in $AgCdVO_4$ [18] and Ag_3PO_4 [19], respectively. In previous work on the compounds $NaMnPO_4$, $Na(Fe, Zn)PO_4$ or $NaCoPO_4$ with the maricite-type structure the sodium atom was considered by the different authors to be in a distorted octahedron NaO_6 with four short and two stretched bonds. This distortion is induced by a displacement of the sodium atom from the centre toward a face of the octahedron. Hammond and Barbier [20] shown by means of bond valence calculation that the coordination sphere of sodium contains at least six oxygen atoms. In the silver compounds $AgMnVO_4$ and $AgCdVO_4$ the first coordination sphere of silver is constituted of four oxygen atoms with distances less than 2.48 Å and the second coordination sphere of six oxygen atoms with distances ranging from 2.94 to 3.22 Å (Table 4). The bond valence calculation confirmed that the silver atom is four coordinated with a BVS value of 0.98 [21]. It means that in these structures the distortion of the octahedra has been achieved and led to four-coordinated silver atoms. This result is in agreement with the fact that silver atoms are known to be stable in low coordination environment [22]. The results of the bond valence calculation for Mn and V confirm that their valences are equal to 2 and 5, respectively (Table 4).

Table 4
Interatomic distances (Å) and bond valence sum (BVS[a]) for $AgMnVO_4$

	Distances	BVS		Distances	BVS
Ag–O3(×2)	2.25(2)		V–O1	1.68(3)	
Ag–O2	2.39(4)		V–O2	1.70(3)	
Ag–O1	2.44(4)		V–O3(×2)	1.72(2)	
Ag–O1	2.94(4)			⟨1.70⟩	5.2(2)
Ag–O3(×2)	3.00(2)				
Ag–O2	3.11(4)		Mn–O3(×2)	2.11(2)	
Ag–O3(×2)	3.21(2)		Mn–O1(×2)	2.22(2)	
	⟨2.33⟩[b]	0.98(4)	Mn–O2(×2)	2.44(3)	
		[C.N. = 4]		⟨2.26⟩	1.82(5)

[a] $BV = e^{(r-r)/b}$ with the following parameters [20]: $b = 0.37$ and $r_0(Ag^I–O) = 1.805$, $r_0(Mn^{II}–O) = 1.790$ and $r_0(V^{+V}–O) = 1.803$.
[b] Average distances are given in brackets.

3.1.2. $RbMnVO_4$

The structure of $RbMnVO_4$ crystallizes with the stuffed-tridymite structure and to our knowledge this is the first vanadate crystallizing with this structural type. The structure can be described as a superposition along the [001] direction of two type of layers *A* and *B* (Fig. 4a). This stacking creates channels where the rubidium atoms are located (Fig. 4b). Layers *A* and *B* are made of two different types of six-membered rings of corner-sharing MnO_4 and VO_4 tetrahedra. Three-fourth of these rings show a UUUDDD (U: up and D: down) topology with the sequence $Mn1O_4$, $V2O_4$, $Mn1O_4$, $V1O_4$, $Mn2O_4$ and $V1O_4$ (Fig. 4c) and one-fourth shows a UDUDUD topology with alternated $Mn1O_4$ and $V1O_4$ tetrahedra (Fig. 4d). The rubidium atoms Rb1 and Rb2 are located in a distorted trigonal prism and a tri-capped octahedron, respectively (Fig. 5).

The Mn–O distances range from 2.009 to 2.032 Å and from 1.995 to 2.016 Å with an average value of 2.026 and 2.000 Å in the $Mn1O_4$ and $Mn2O_4$ tetrahedra, respectively. These values are lower than the expected value of 2.04 Å calculated from the Shannon table [23]. This explains the overbonding of the manganese atoms reflected by the BVS of 2.11 and 2.27 for Mn1 and Mn2, respectively (Table 5). The average distances in VO_4 tetrahedra of 1.713 and 1.710 Å for V1–O and V2–O, respectively are lower than the sum of the ionic radii 1.735 Å and as observed for manganese atoms the vanadium atoms are also slightly overbonded (Table 5). In the $Rb1O_6$ trigonal prism the Rb1–O distance range from 2.840 to 3.207 Å with an average value of 2.983 Å and a BVS of 0.923. In the $Rb2O_9$ tri-capped octahedra the Rb2–O distances range from 3.016 to 3.318 Å with an average value of 3.158 and a BVS of 0.846 indicating a slightly under-bonded Rb2 position.

3.2. Magnetic susceptibility and specific heat measurements

3.2.1. $AgMnVO_4$

The magnetic susceptibility χ versus *T* and the corresponding χ^{-1} versus *T* for $AgMnVO_4$ are shown in Fig. 6. The χ^{-1} versus *T* plot reveals that $AgMnVO_4$ exhibits a paramagnetic behaviour in the temperature range 70–340 K. A small jump in the susceptibility curve is observed around 220 K and this may arise from the

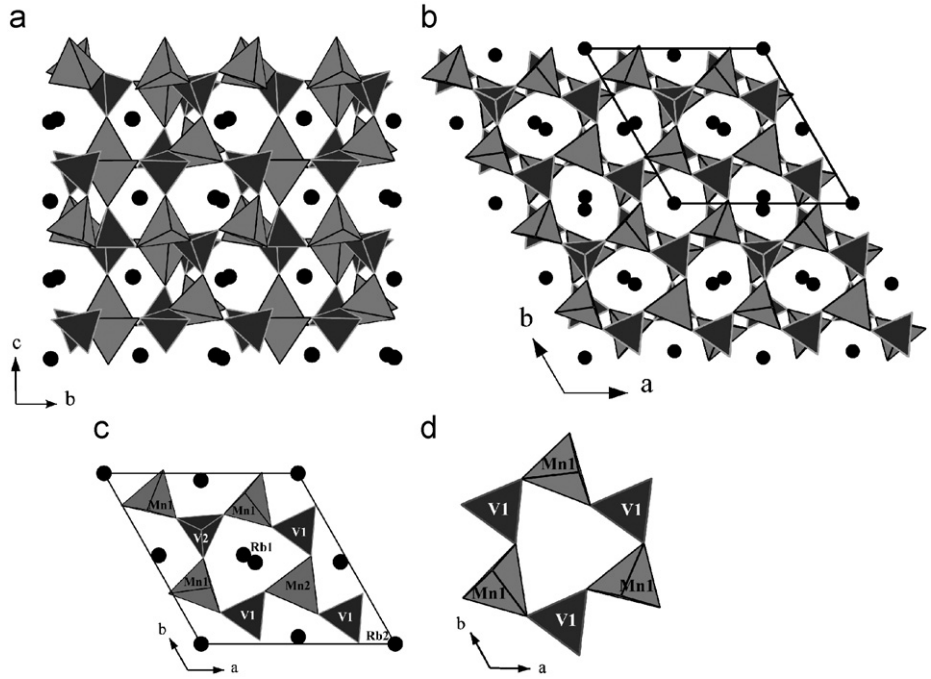

Fig. 4. Structure of $RbMnVO_4$: (a) staking of layers *A* and *B* constituted of six-membered rings. (b) Projection of the structure on (001). (c) Topology UUUDDD of the first type of six-membered ring with alternation of MnO_4 and VO_4 tetrahedra. (d) Topology UDUDUD of the second type of six-membered ring with alternation of MnO_4 and VO_4 tetrahedra.

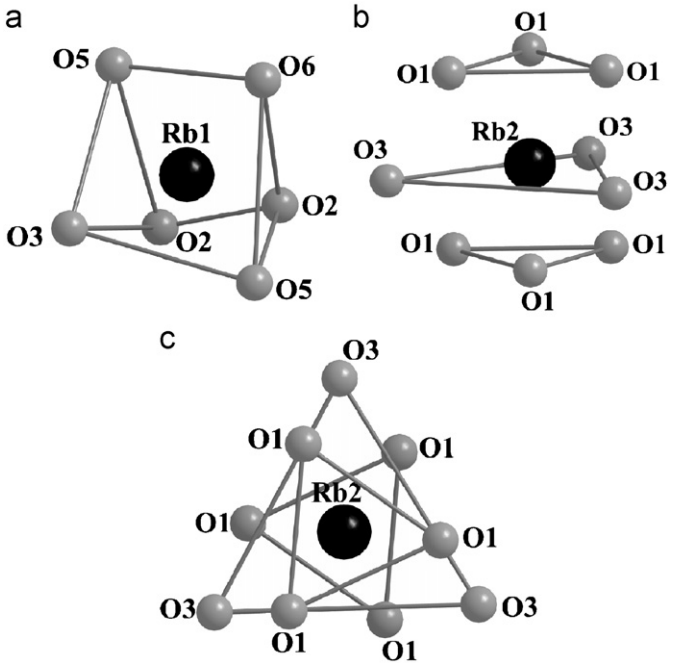

Fig. 5. Perspective view of (a) the $Rb1O_6$ distorted prism, (b) the ninth-coordinated Rb2 position and (c) a projection view of $Rb2O_9$ along [001].

Table 5
Interatomic distances (Å), bond valence (BV^a) and bond valence sum (BVS) for $RbMnVO_4$

	Distances	BV		Distances	BV
Rb1–O6	2.840(7)	0.210	Mn2–O3	1.995(8)	0.575
Rb1–O2	2.842(8)	0.209	Mn2–O2	1.988(6)	0.586
Rb1–O3	2.898(7)	0.180	Mn2–O1	2.000(9)	0.567
Rb1–O5	2.948(7)	0.157	Mn2–O6	2.016(9)	0.543
Rb1–O2	3.160(10)	0.089		〈2.000〉	BVS = 2.27(3)
Rb1–O5	3.207(8)	0.078			
	〈2.983〉[b]	BVS = 0.923(8)	V1–O1	1.698(9)	1.328
			V1–O3	1.716(9)	1.265
Rb2–O1 (× 3)	3.016(9)	0.131	V1–O5	1.719(6)	1.255
Rb2–O1 (× 3)	3.139(9)	0.094	V1–O6	1.719(8)	1.255
Rb2–O3 (× 3)	3.318(11)	0.058		〈1.713〉	BVS = 5.10(6)
	〈3.158〉	BVS = 0.846(6)			
			V2–O4	1.680(12)	1.394
Mn1–O4	2.009(12)	0.553	V2–O2 (× 3)	1.720(12)	1.251
Mn1–O5 (× 3)	2.032(12)	0.520		〈1.710〉	BVS = 5.15(7)
	〈2.026〉	BVS = 2.11(3)			

[a] $BV = e^{(r_0-r)/b}$ with the following parameters [20]: $b = 0.37$ and r_0 (Mn^{II}–O) = 1.790, $r_0(V^{+V}–O) = 1.803$ and $r_0(Rb^{+I}–O) = 2.263$.
[b] Average distances are given in brackets.

structural transition of $Mn_2V_2O_7$ [24,25]. This observation is in agreement with the analysis of the powder pattern (Fig. 1). The susceptibility above 70 K follows a Curie–Weiss law with $\theta = -62(1)$ K and $C = 4.44\,mol^{-1}\,cm^3\,K$. The effective magnetic moment calculated from the Curie constant $\mu_{eff} = 5.96(1)\,\mu_B$ is close to the spin-only value of 5.92 μ_B expected for a high-spin Mn^{2+} (d^5) ion. A local maximum of the susceptibility is observed at $T_{max} = 24$ K and a local minimum at 12 K followed by an increase toward low temperatures. The negative value of θ indicates that the predominant interactions between Mn^{2+} ions are antiferromagnetic. The specific heat of $AgMnVO_4$ exhibits a lambda-type anomaly at 12.30(2) K which corresponds to the Néel temperature (Fig. 7). This temperature corresponds exactly to the local minimum in the susceptibility curve at 12 K. One can notice that on the specific curve a very small peak is also observed at 20 K which corresponds to the T_N of $Mn_2V_2O_7$. In the light of a previous study on $CuMnVO_4$ showing the same type of infinite Mn–Mn chains, an explanation of the susceptibility behaviour can be proposed [8]. The Néel temperature $T_N = 12.3$ K does not correspond to the maximum of the susceptibility observed at

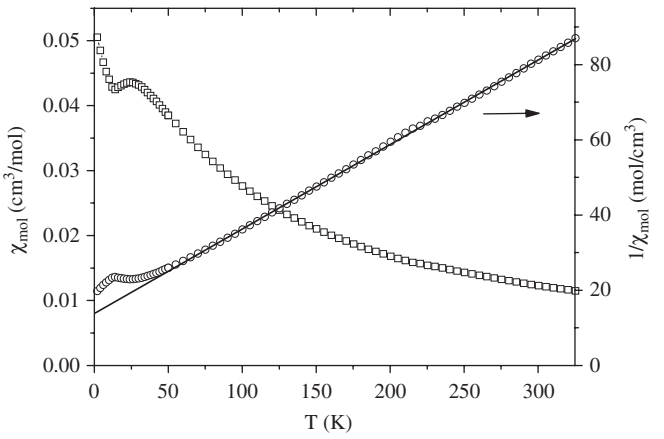

Fig. 6. Magnetic susceptibility χ versus temperature and the corresponding χ^{-1} versus T plots of $AgMnVO_4$ measured with the applied field $H = 5$ kOe.

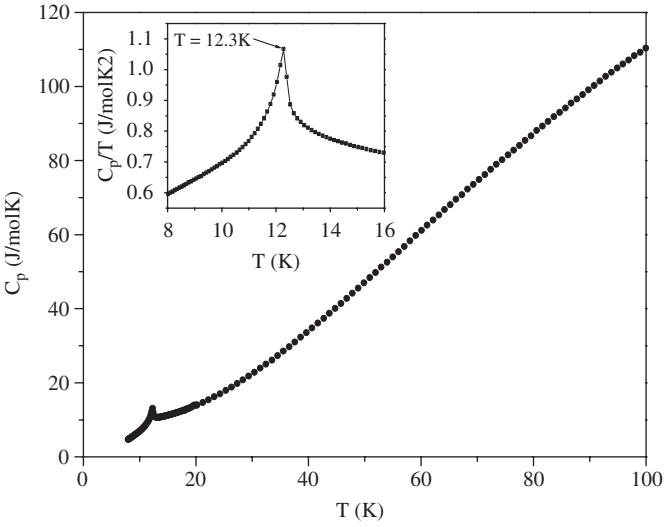

Fig. 7. The specific heat C_p versus T plot of $AgMnVO_4$. The inset displays C_p/T in the region of the magnetic transition at 12.3 K.

$T_{max} = 24$ K and this implies low-dimensional magnetic properties of $AgMnVO_4$. $T_{max} = 24$ K is characteristic of the Mn–Mn exchange interactions within the linear chains parallel to [010] (Fig. 3a). The strong susceptibility increase below 12 K may be attributed to traces of paramagnetic impurities.

3.2.2. $RbMnVO_4$

The molar magnetization σ versus H for the polycrystalline sample of $RbMnVO_4$ at different temperature is presented in Fig. 8. It appears clearly that at $T = 2$ K, the variation of the molar magnetization is not linear at low fields and do not saturate in strong fields. This behaviour is characteristic of a canted antiferromagnetism where the spins of two (or more) sublattices are not antiparallel but slightly tilted or 'canted' out of alignment. The result is a small net magnetization σ_s in one direction. At high fields, the magnetization do not saturate and a susceptibility χ_{mol} appropriate to the basic antiferromagnetism can be deduced. The magnetization curve for a given temperature below the Néel temperature can be described by $\sigma_{mol} = \sigma_s + \chi_{mol}H$. At $T = 2$ K, σ_s is close to 0.15 μ_B (Fig. 8). Obviously, above the Néel temperature the magnetization versus H is linear. For $RbMnVO_4$, the magnetization is linear for all the values of magnetic field for $T \geqslant 8$ K (Fig. 8). Therefore, the Néel temperature has been estimated at ~8 K.

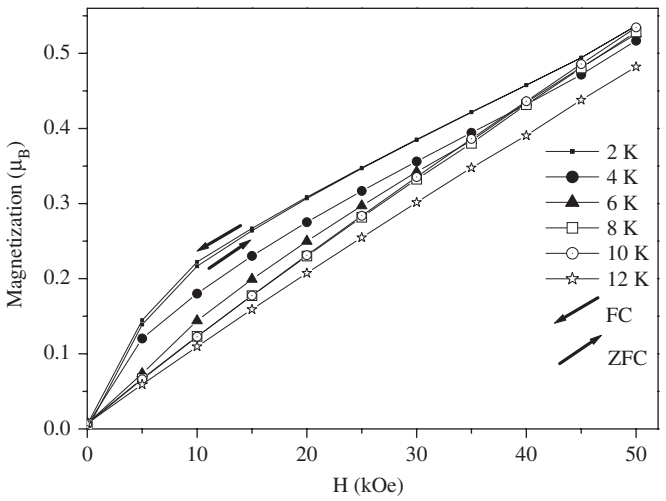

Fig. 8. Magnetization as function of field at different temperatures for $RbMnVO_4$.

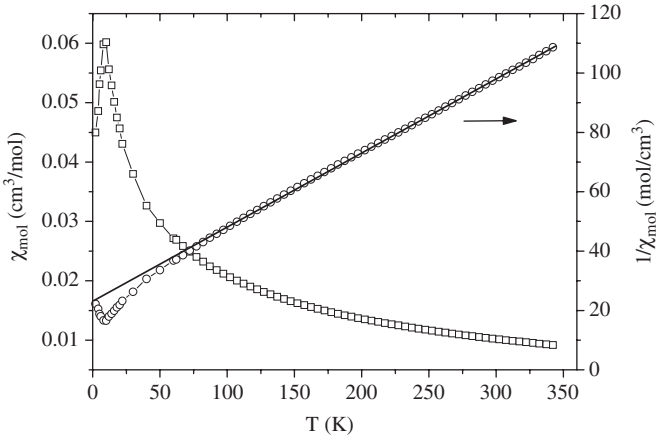

Fig. 9. Magnetic susceptibility χ versus temperature and χ^{-1} versus T plots for $RbMnVO_4$.

In the range 2–60 K the susceptibility values were deduced from the slope of the $\sigma_{mol} = f(H)$ curves at $H = 5$ kOe and above 60 K directly from the magnetization values measured at the same field. This molar magnetic susceptibility χ_{mol} versus T and the corresponding χ^{-1}_{mol} versus T are shown in Fig. 9. The susceptibility above 80 K follows a Curie–Weiss law with $\theta = -93(1)$ K which indicates a predominant antiferromagnetic interaction between adjacent Mn^{2+} ions and $C = 4.01(2)\,mol^{-1}\,cm^3\,K$. The effective magnetic moment μ_{eff} calculated from the Curie constant is equal to 5.67(1) μ_B and is slightly lower than the value expected for a high-spin Mn^{2+} (d^5) ion ($\mu_{spin\text{-}only} = 5.92\,\mu_B$). The Néel temperature corresponding to the maximum of the susceptibility is close to 8 K (Fig. 9). This result has been confirmed by heat capacity measurement between 2 and 100 K (Fig. 10). A λ-type anomaly associated with the 3D magnetic transition is observed at $T = 6.5$ K (see inset). The reciprocal susceptibility between 7 and 80 K deviates clearly from the Curie–Weiss law with a small ferromagnetic component (Fig. 9). This behaviour is coherent with a canted antiferromagnetic magnetic structure of $RbMnVO_4$.

The canting of the spins was first realized by Dzialoshinsky [26] in a phenomenological study of α-Fe_2O_3 and put on a firm theoretical basis by Moriya [27]. The main rule to canting to occur is a symmetry restriction where the magnetic moments in a unit cell cannot be related by a centre of symmetry. We can notice that the space group of $RbMnVO_4$ ($P6_3$) satisfies this condition. It is

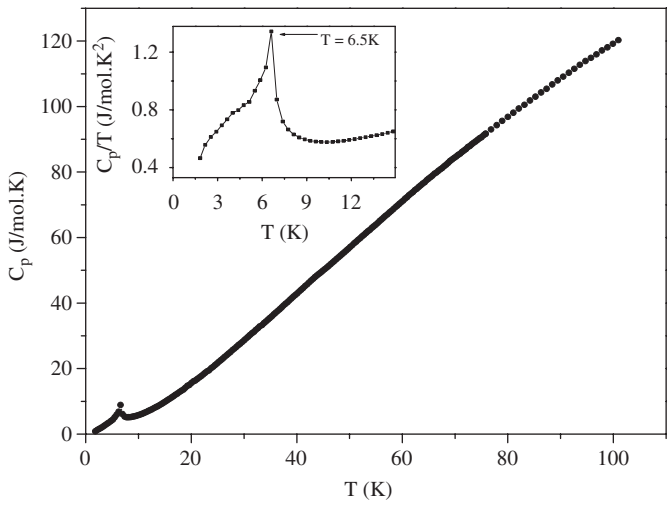

Fig. 10. The specific heat C_p versus T plot of $RbMnVO_4$. The inset displays C_p/T in the region of the magnetic transition at 6.5 K.

obvious that the determination of the magnetic structure of $RbMnVO_4$ would be very useful to confirm that $RbMnVO_4$ is a canted antiferromagnet.

4. Conclusions

The $AMnVO_4$ series has been extended with the new vanadates $AgMnVO_4$ and $RbMnVO_4$ and now is known for $A =$ Li, K, Rb, Cu, Ag. $AgMnVO_4$ crystallizes with a maricite-type structure and $RbMnVO_4$ with a stuffed-tridymite structure. $RbMnVO_4$ is the first vanadate crystallizing with this structural type. From a structural point of view the $AMnPO_4$ and $AMnVO_4$ series show significant differences. Indeed, except for $AgMnVO_4$ and $NaMnPO_4$ which both crystallize with a maricite-type structure all the others compounds crystallize with a different structural type. When phosphates crystallize with the olivine or zeolite-ABW structure type, the vanadates crystallize with the Na_2CrO_4, perovskite or stuffed-tridymite structure type. Concerning the magnetic properties, antiferromagnetic interactions between the Mn^{2+} ions are observed for all vanadate compounds.

Appendix A. Supplementary materials

Supplementary data associated with this article can be found in the online version at doi:10.1016/j.jssc.2008.08.001.

References

[1] S. Geller, J.L. Durand, Acta Crystallogr. 13 (1960) 325–331.
[2] J. Moring, E. Kostiner, J. Solid State Chem. 61 (1986) 379–383.
[3] M. Lujan, F. Kubel, H. Schmid, Z. Naturforsch. 50b (1995) 1210–1214.
[4] O.V. Yakubovich, M.A. Simonov, O.K. Mel'nikov, Kristallografiya 35 (1990) 42–46.
[5] H. Ben Yahia, E. Gaudin, J. Darriet, J. Alloys Compd. 442 (2007) 74–76.
[6] A.K. Padhi, W.B. Archibald, K.S. Nanjundaswamy, J.B. Goodenough, Solid State Chem. 128 (1997) 267–272.
[7] S.-Y. Chung, J.T. Bloking, Y.-M. Chiang, Nat. Mater. 1 (2002) 123–128.
[8] H.B. Yahia, E. Gaudin, J. Darriet, M. Banks, R.K. Kremer, A. Villesuzanne, M.H. Whangbo, Inorg. Chem. 44 (9) (2005) 3087–3093.
[9] H. Ben Yahia, E. Gaudin, C. Lee, M.H. Whangbo, J. Darriet, Chem. Mater. 19 (2007) 5563–5569.
[10] H. Ben Yahia, E. Gaudin, J. Darriet, Z. Naturforsch. 62b (2007) 873–880.
[11] A. Boultif, D. Louer, J. Appl. Crystallogr. 37 (2004) 724–731.
[12] V. Petricek, M. Dusek, L. Palatinus, Jana2000. The Crystallographic Computing System, Institute of Physics, Praha, Czech Republic, 2000.
[13] J.F. Bérar, G. Baldinozzi, J. Appl. Crystallogr. 26 (1993) 128–129.
[14] F.E. Mabbs, D.J. Machin, Magnetism and Transition Metal Complexes, Chapman & Hall, London, 1973.
[15] A. Altomare, M.C. Burla, M. Camalli, G.L. Cascarano, C. Giacovazzo, A. Guagliardi, A.G.G. Moliterni, G. Polidori, R. Spagna, J. Appl. Crystallogr. 32 (1999) 115–119.
[16] V. Kahlenberg, R.X. Fischer, J.B. Parise, J. Solid State Chem. 154 (2000) 612–618.
[17] E. Gaudin, V. Petricek, F. Boucher, F. Taulelle, M. Evain, Acta Crystallogr. B 56 (2000) 972–979.
[18] S. Muenchau, H. Mueller-Buschbaum, Z. Naturforsch. B: Chem. Sci. 50 (1995) 703–706.
[19] H.N. Ng, C. Calvo, R. Faggiani, Acta Crystallogr. B 34 (1978) 898–899.
[20] R. Hammond, J. Barbier, Acta Crystallogr. B 52 (1996) 440–449.
[21] I.D. Brown, D. Altermatt, Acta Crystallogr. B 41 (1985) 244–247.
[22] E. Gaudin, F. Boucher, M. Evain, J. Solid State Chem. 160 (2001) 212–221.
[23] R.D. Shannon, Acta Crystallogr. A 32 (1976) 751–761.
[24] Z. He, Y. Ueda, J. Solid State Chem. 181 (2008) 235–238.
[25] Z. He, Y. Ueda, M. Itoh, Solid State Commun. 147 (2008) 138–140.
[26] I. Dzyaloshinsky, J. Phys. Chem. Solids 4 (1958) 241–255.
[27] T. Moriya, Phys. Rev. 117 (1960) 635–647.